6-2011

Photoisomerization of Stilbene: A Spin-Flip Density Functional Theory Approach

Noriyuki Minezawa
Iowa State University

Mark S. Gordon
Iowa State University, mgordon@iastate.edu

Photoisomerization of Stilbene: A Spin-Flip Density Functional Theory Approach

Abstract

The photoisomerization process of 1,2-diphenylethylene (stilbene) is investigated using the spin-flip density functional theory (SFDFT), which has recently been shown to be a promising approach for locating conical intersection (CI) points (Minezawa, N.; Gordon, M. S. *J. Phys. Chem. A***2009**, *113*, 12749). The SFDFT method gives valuable insight into twisted stilbene to which the linear response time-dependent DFT approach cannot be applied. In contrast to the previous SFDFT study of ethylene, a distinct twisted minimum is found for stilbene. The optimized structure has a sizable pyramidalization angle and strong ionic character, indicating that a purely twisted geometry is not a true minimum. In addition, the SFDFT approach can successfully locate two CI points: the twisted-pyramidalized CI that is similar to the ethylene counterpart and another CI that possibly lies on the cyclization pathway of *cis*-stilbene. The mechanisms of the cis–trans isomerization reaction are discussed on the basis of the two-dimensional potential energy surface along the twisting and pyramidalization angles.

Disciplines

Chemistry

Comments

Reprinted (adapted) with permission from *Journal of Physical Chemistry A* 115 (2011): 7901, doi:10.1021/jp203803a.

THE JOURNAL OF PHYSICAL CHEMISTRY A

ARTICLE

pubs.acs.org/JPCA

Photoisomerization of Stilbene: A Spin-Flip Density Functional Theory Approach

Noriyuki Minezawa and Mark S. Gordon*

Department of Chemistry, Iowa State University, Ames, Iowa 50011, United States

Supporting Information

ABSTRACT: The photoisomerization process of 1,2-diphenylethylene (stilbene) is investigated using the spin-flip density functional theory (SFDFT), which has recently been shown to be a promising approach for locating conical intersection (CI) points (Minezawa, N.; Gordon, M. S. *J. Phys. Chem. A* **2009**, *113*, 12749). The SFDFT method gives valuable insight into twisted stilbene to which the linear response time-dependent DFT approach cannot be applied. In contrast to the previous SFDFT study of ethylene, a distinct twisted minimum is found for stilbene. The optimized structure has a sizable pyramidalization angle and strong ionic character, indicating that a purely twisted geometry is not a true minimum. In addition, the SFDFT approach can successfully locate two CI points: the twisted-pyramidalized CI that is similar to the ethylene counterpart and another CI that possibly lies on the cyclization pathway of *cis*-stilbene. The mechanisms of the cis−trans isomerization reaction are discussed on the basis of the two-dimensional potential energy surface along the twisting and pyramidalization angles.

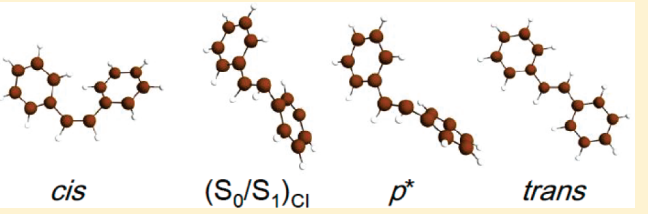

1. INTRODUCTION

The cis−trans isomerization reaction is a fundamental process in photochemistry. 1,2-Diphenylethylene (stilbene) is a prototypical molecule that undergoes photoisomerization,[1,2] and the molecule has been extensively investigated by both experimental[3−36] and theoretical[37−65] approaches. Stilbene photoisomerization takes place in both the cis-to-trans and trans-to-cis directions. It has been generally accepted that the relaxation of both cis and trans isomers involves the central C═C bond twisting motion toward the perpendicular conformation (so-called phantom state[18,25]) on the excited-state potential energy surface (PES). A conical intersection (CI)[66−70] apparently exists near the twisted minimum. Since the CI acts as a funnel connecting multiple electronic states, the photoexcited stilbene is allowed to return to the ground state with a rapid internal conversion. On the ground state PES, some molecules complete the twisting motion and lead to the product, and others return to the initial isomer (reactant). The cis and trans isomers are produced in approximately equal amounts, whether the reactant is *cis*- or *trans*-stilbene. However, there are some striking differences between the cis-to-trans and trans-to-cis isomerization processes. First, the isomerization proceeds much faster in the former (∼2 ps)[7,8,11,14,16,18,24,25,27,32] than in the latter (10−200 ps).[9,10,24,25,36] The experiments illustrate that there is a relatively large barrier (∼3 kcal/mol) on the trans-to-cis isomerization path,[3,4,6,31] while the cis-to-trans reaction involves a negligible barrier or a barrierless process.[17,24,27,30,34] Second, in the *cis*-stilbene isomerization reaction, a cyclization product, 4a,4b-dihydrophenanthrene (DHP), is observed along with the trans isomer product, although the experimental quantum yield is relatively small (0.10) compared to that of the trans isomer (0.35).[40,71] The byproduct formation indicates that another reaction channel is open for the cis isomer.

To provide insight into the mechanisms of photoisomerization in stilbene, it is necessary to apply quantum mechanical methods that can describe not only the relevant excited-state minimum energy points but also the conical intersections. Because the excited-state lifetime and product yield are closely related to the location of the CI points, an accurate description of the CI point energy and geometries is of the utmost importance. The state-averaged complete active space self-consistent field (SA-CASSCF) method has been widely applied to explore the excited-state PES because the analytic gradient and derivative coupling vectors are available to specify the CI seam. To optimize the CI points with methods that account for dynamic correlation, which is missing at the SA-CASSCF level, the derivative coupling expression has been derived and implemented for multireference configuration interaction (MR-CI)[72,73] and multistate second-order perturbation theory for the SA-CASSCF reference (MS-CASPT2)[74] methods. CI searches by these correlated methods indicate that dynamic electron correlation significantly modifies the PES and geometries in the region of the CI points.

Time-dependent density functional theory (TDDFT)[75−77] is an alternative approach to take into account dynamic correlation effects for describing electronically excited states. The linear response (LR) TDDFT approach has been applied successfully to compute the absorption and fluorescence spectra of large molecular systems, and LR-TDDFT has been combined with

Received: April 24, 2011
Revised: June 1, 2011
Published: June 03, 2011

nonadiabatic molecular dynamics simulations[78−85] to examine the relaxation pathways of photoexcited molecules. However, the applicability of LR-TDDFT to CI points is questionable for several reasons.[86] First, a single-reference theory has difficulty in describing CI points because of the multiconfigurational character in these regions of a PES. Second, in the vicinity of CI points, LR-TDDFT gives too rapid a change in the potential energy curves. In addition, the response state can become lower in energy than that of the reference state. Levine et al.[86] have discussed these LR-TDDFT failures in the CI optimization of twisted ethylene and suggested the possibility of a spin-flip TDDFT (or simply "SFDFT") approach[87−92] to locate CI points. While spin-flip approaches have been applied mainly to describe low-lying singlet and triplet states for biradicals,[93] the SFDFT method is also useful in that the CI points of ethylene can be successfully located and that the resultant energies and geometries are comparable to those obtained by the MR-CI and MS-CASPT2 methods.[94] In contrast to the conventional LR-TDDFT method, SFDFT employs the triplet $\alpha\alpha(M_S = +1)$ state as the reference and allows only $\alpha \rightarrow \beta$ spin-flipped excitations. It is the doubly excited $\pi^*_\alpha\pi^*_\beta$ configuration that accounts for the stabilization of ethylene along the pyramidalization angle. The doubly excited configuration is naturally taken into account by a single spin-flip excitation from the triplet $\pi_\alpha\pi^*_\alpha$ reference, while the conventional LR-TDDFT cannot describe the double excitation at all. Furthermore, the SFDFT approach treats both the S_0 and S_1 states on an equal footing as the response states, while the S_0 state is always the reference state in LR-TDDFT. Therefore, the SFDFT approach is superior to the LR-TDDFT method in describing CI points.

In the present work, the SFDFT method is applied to examine the photochemistry of stilbene. Because stilbene may be thought of as a substituted ethylene, it is expected that the SFDFT method is a promising approach to describe the CI points and that the LR-TDDFT method will suffer from the same problems observed in ethylene.[86] Although the recent study by Huix-Rotllant et al. has pointed out that SFDFT has some difficulty in describing CI points when three nearly degenerate orbitals appear in the vicinity of the CI points,[95] the photoisomerization around the C═C bond is well described by two orbitals (π and π^*).

Following a presentation of the theoretical and computational methods used here, the excited-state minimum and CI points are discussed. The perpendicular structure gives particularly valuable insight into the mechanism of cis−trans photoisomerization. In addition, the present SFDFT approach can access the twisted stilbene species, whereas the previous LR-TDDFT study was unable to access this structure.[53,55] By using a penalty-constrained optimization method,[86,96] SFDFT can successfully locate the two CI points of stilbene: the twisted-pyramidalized CI observed also in the previous SFDFT study of ethylene[94] and another CI point which possibly lies on the cyclization reaction path. The relationship between the CI and minimum energy points is discussed. Interestingly, Levine et al.[96] have shown that the twisted-pyramidalized CI geometry optimized by the MS-CASPT2 method leads to the global minimum of the S_1 state, while the SA-CASSCF method has a distinctly different minimum. Therefore, it is important to take into account dynamic correlation effects in optimizing the geometries for both the CI point and the excited-state minima.

Second, the full two-dimensional PES for the S_1 state is constructed along the central C═C twisting motion and the pyramidalization angle. These two coordinates play an important role in the photoisomerization of stilbene, although it is conceivable that other coordinates participate in the dynamics.[18,19] The isomerization of both cis-to-trans and trans-to-cis processes is examined on the basis of the computed PES.

2. METHODS AND COMPUTATIONAL DETAILS

2.1. Spin-Flip TDDFT. Within the linear-response TDDFT approach,[76] the excitation energy Ω and transition amplitudes $\mathbf{X}$ and $\mathbf{Y}$ are obtained by solving the non-Hermitian equation

$$\begin{pmatrix} \mathbf{A} & \mathbf{B} \\ \mathbf{B} & \mathbf{A} \end{pmatrix} \begin{pmatrix} \mathbf{X} \\ \mathbf{Y} \end{pmatrix} = \Omega \begin{pmatrix} 1 & 0 \\ 0 & -1 \end{pmatrix} \begin{pmatrix} \mathbf{X} \\ \mathbf{Y} \end{pmatrix} \tag{1}$$

The coupling matrices $\mathbf{A}$ and $\mathbf{B}$ are given as follows

$$\begin{aligned} A^{\mathrm{TDDFT}}_{ia,jb} &= (\varepsilon_a - \varepsilon_i)\delta_{ij}\delta_{ab} + \langle ij|ab\rangle - c_x\langle ia|jb\rangle + \langle ij|f^{\mathrm{xc}}|ab\rangle \\ B^{\mathrm{TDDFT}}_{ia,jb} &= \langle ij|ab\rangle - c_x\langle ij|ba\rangle + \langle ij|f^{\mathrm{xc}}|ab\rangle \end{aligned} \tag{2}$$

where

$$\langle pq|rs\rangle = \iint \mathrm{d}\mathbf{r}_1\mathrm{d}\mathbf{r}_2\psi^*_p(\mathbf{r}_1)\psi^*_q(\mathbf{r}_2)\frac{1}{r_{12}}\psi_r(\mathbf{r}_1)\psi_s(\mathbf{r}_2) \tag{3}$$

$$\langle pq|f^{\mathrm{xc}}|rs\rangle = \iint \mathrm{d}\mathbf{r}_1\mathrm{d}\mathbf{r}_2\psi^*_p(\mathbf{r}_1)\psi^*_q(\mathbf{r}_2)f^{\mathrm{xc}}(\mathbf{r}_1,\mathbf{r}_2)\psi_r(\mathbf{r}_1)\psi_s(\mathbf{r}_2) \tag{4}$$

The labels i, j, ... and a, b, ... refer to occupied and virtual molecular orbitals (MOs), respectively. $\{\varepsilon_i, \varepsilon_a\}$ are the orbital energies, and c_x is a mixing weight of the Hartree−Fock exchange integral in the hybrid functional. The exchange-correlation kernel, f^{xc}, is given by the second functional derivative of the exchange-correlation energy.

In the SFDFT method, the triplet state that has two unpaired alpha electrons is chosen as the reference state. Note that the occupied and virtual orbitals are defined according to the occupation number in this reference triplet state. In ethylene, for example, the reference is the triplet $\pi_\alpha\pi^*_\alpha$ state, and π_α and π^*_α belong to the occupied space and π_β and π^*_β to the virtual space. To provide a correct description of the singlet states that have an equal number of alpha and beta electrons, only the spin-flipped block, that is, the excitation from the occupied alpha orbital to virtual beta orbital, is allowed to be nonzero in the coupling matrices. Taking into account the spin orthogonality between the occupied alpha and virtual beta orbitals, the SFDFT coupling matrix elements are given by

$$\begin{aligned} A^{\mathrm{SFDFT}}_{ia,jb} &= (\varepsilon_a - \varepsilon_i)\delta_{ij}\delta_{ab} - c_x\langle ia|jb\rangle \\ B^{\mathrm{SFDFT}}_{ia,jb} &= 0 \end{aligned} \tag{5}$$

Here, the collinear exchange-correlation functional is assumed, i.e., $\langle ij|f^{\mathrm{xc}}|ab\rangle = 0$. The SFDFT equations presented above are identical with the original formulation in ref 87. The resultant SFDFT excitation energy Ω and transition amplitude $\mathbf{X}$ are obtained by solving the following Hermitian matrix equation

$$\mathbf{AX} = \Omega\mathbf{X} \tag{6}$$

Although setting $\mathbf{B} = 0$ is known as the Tamm−Dancoff approximation in the LR-TDDFT method, the coupling matrix

B is exactly zero within the framework of the collinear SFDFT method. The SFDFT method has recently been developed in several directions. A noncollinear formulation has been introduced to describe the exchange-correlation functional.[88−91,95] Wang and Ziegler[88] and Vahtras and Rinkevicius[90] have formulated a general framework within the TDDFT approach to treat the transitions from a nonsinglet ground state to excited states with arbitrary spin multiplicity. Very recently, Rinkevicius and Ågren[91] have described the reference state using a restricted open shell method rather than the unrestricted SCF approach adopted in the present work.

2.2. Penalty-Constrained Optimization Method. To locate a CI point between states I and J, a penalty-constrained optimization approach[86,96] is adopted. The method requires the minimization of the following objective functions

$$f(\mathbf{R},\sigma) = \bar{E}_{IJ}(\mathbf{R}) + \sigma G_{IJ}(\mathbf{R}) \quad (7)$$

The first term expresses the average potential energy of the two states.

$$\bar{E}_{IJ}(\mathbf{R}) = \frac{E_I(\mathbf{R}) + E_J(\mathbf{R})}{2} \quad (8)$$

The second term is the product of the Lagrange multiplier, σ, and the penalty term

$$G_{IJ}(\mathbf{R}) = \frac{[E_I(\mathbf{R}) - E_J(\mathbf{R})]^2}{E_I(\mathbf{R}) - E_J(\mathbf{R}) + \alpha} \quad E_I(\mathbf{R}) \geq E_J(\mathbf{R}) \quad (9)$$

where the state I is taken to be the upper state. The smoothing parameter α is introduced to ensure the differentiability of eq 9 in the neighborhood of CI points. As discussed in ref 96, three criteria are employed to achieve the convergence of eq 7: the change in the objective function f between the m-th and $(m+1)$-th optimization steps must be less than a tolerance, $\mathrm{tol}_{\mathrm{step}}$

$$|f(\mathbf{R}_m,\sigma) - f(\mathbf{R}_{m+1},\sigma)| \leq \mathrm{tol}_{\mathrm{step}} \quad (10)$$

and the parallel and perpendicular components of the gradient of f with respect to the direction of the gradient vector of the penalty must be less than the tolerance $\mathrm{tol}_{\mathrm{grad}}$

$$|\hat{\mathbf{u}}\cdot\nabla_{\mathbf{R}} f(\mathbf{R},\sigma)| \leq \mathrm{tol}_{\mathrm{grad}} \quad (11)$$

$$|\nabla_{\mathbf{R}} f(\mathbf{R},\sigma) - \hat{\mathbf{u}}\cdot\nabla_{\mathbf{R}} f(\mathbf{R},\sigma)| \leq \mathrm{tol}_{\mathrm{grad}} \quad (12)$$

where

$$\hat{\mathbf{u}} = \frac{\nabla_{\mathbf{R}} G(\mathbf{R})}{|\nabla_{\mathbf{R}} G(\mathbf{R})|} \quad (13)$$

The three criteria are minimized simultaneously to be lower than their respective thresholds, $\mathrm{tol}_{\mathrm{step}}$ and $\mathrm{tol}_{\mathrm{grad}}$. The objective function f is minimized with fixed σ until eqs 10−12 are satisfied. Hence, the resultant energies and geometries depend parametrically on σ. If the energy gap between the two states is larger than the threshold ε

$$E_I(\mathbf{R};\sigma) - E_J(\mathbf{R};\sigma) \geq \varepsilon \quad (14)$$

then the Lagrange multiplier σ is increased, and the optimization is restarted. The parameter σ is increased until the energy difference between the two states becomes less than the given value of ε.

The PESs around the CI point are often described using the branching space (**g**−**h** plane) introduced by Yarkony.[69,70] In the penalty-constrained method, however, the near-degeneracy region of the two surfaces is explored just by imposing the penalty. The algorithm uses only the gradient difference (**g**) that is slightly modified according to eq 9, while the second vector, i.e., the interstate coupling vector (**h**), never appears. The validity of the CI search algorithm has been discussed in ref 96.

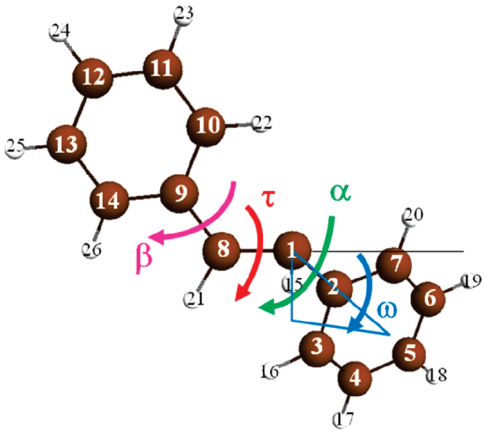

Figure 1. Coordinate system of stilbene. Some important angles are also shown: C=C twisting angle (τ), pyramidalization angle (ω), and the phenyl-group twisting angles around the C_1-C_2 (α) and C_8-C_9 (β) bonds.

2.3. Computational Details. The SFDFT energy and analytic gradient were implemented in the electronic structure code GAMESS (General Atomic and Molecular Electronic Structure System).[97,98] The BHHLYP hybrid functional (50% Hartree−Fock plus 50% Becke exchange[99] with Lee−Yang−Parr correlation[100]) was employed in the present work because the collinear SFDFT benchmark calculations suggest that one will obtain better performance with a larger fraction of Hartree−Fock exchange.[87,94] This is due to the fact that only the Hartree−Fock exchange term contributes to the off-diagonal element of the coupling matrix, eq 5, within the collinear exchange-correlation approximation. The long-range correction, range-separated functionals, and noncollinear functionals may affect the CI geometries and energies, and these points should be examined in future work. The basis set employed was the Dunning−Hay double-ζ plus polarization DH(d,p) basis.[101] The PES of stilbene was constructed as a function of the twisting and pyramidalization angles (see Figure 1). The central C_1-C_8 bond twisting angle τ was defined as the average of four dihedral angles, $C_2C_1C_8C_9$, $C_2C_1C_8H_{21}$, $H_{15}C_1C_8C_9$, and $H_{15}C_1C_8H_{21}$, and the planar cis (trans) conformation corresponds to τ = 0° (180°). Similarly, the phenyl ring twisting angles, α and β, are defined as the average of four dihedral angles around the C_1-C_2 and C_8-C_9 bonds, respectively. The pyramidalization angle ω is defined as the C_8 atom bending out of the $C_1C_2H_{15}$ plane. For the S_1 state, the geometries were determined by optimizing the remaining degrees of freedom at given values of τ and ω. At the energy minimum points, all vibrational frequencies were computed to be positive, and the zero point energy (ZPE) correction was added without scaling. In the CI point search, the Broyden−Fletcher−Goldfarb−Shannon (BFGS) quasi-Newton scheme was adopted to minimize the objective function in eq 6. The parameters in eqs 9−13 were taken from ref 96: the smoothing parameter α was 0.02 hartree, and the CI search criteria, $\mathrm{tol}_{\mathrm{step}}$ and $\mathrm{tol}_{\mathrm{grad}}$, were set to be 10^{-6} hartree and 0.0005 hartree/bohr,

dx.doi.org/10.1021/jp203803a |J. Phys. Chem. A 2011, 115, 7901–7911

respectively. The maximum acceptable energy gap ε was 10^{-3} hartree. No symmetry constraint was applied during the geometry optimizations.

3. RESULTS AND DISCUSSION

In this section, the results of the SF-BHHLYP calculations for stilbene are presented. First, the ground-state geometries and vertical excitation energies are discussed. Next, the geometries are optimized at the excited-state energy minima and CI points, and the geometric parameters are compared to those of the previous calculations with the SA-2-CAS(2,2)/6-31G (two-state average CASSCF with the active space consisting of two electrons in two orbitals),[47] SA-3-CAS(2,2)/6-31G(d,p),[96] and MS-CASPT2/6-31G(d,p) with a SA-3-CAS(2,2) reference[96] (simply MS-CASPT2 hereafter) methods. Finally, the trans-to-cis and cis-to-trans isomerization reactions are examined on the basis of the S_1 PES and relevant CI points.

3.1. Ground State. Figure 2 shows the SF-BHHLYP ground-state optimized geometries for the cis and trans isomers, $(S_0)_{cis}$ and $(S_0)_{trans}$, respectively. The optimized geometric parameters are in good agreement with the results of the previous calculations[43−45,47,51,53] and the gas-phase electron diffraction experiments[102,103] though there is some discrepancy in the phenyl rotation of *trans*-stilbene. The $(S_0)_{trans}$ structure has approximately C_{2h} symmetry and has a molecular plane, and the phenyl-ring twisting angles, α and β, are nearly 0°. The planarity of *trans*-stilbene, however, has been a source of controversy.[104,105] The SA-2-CAS(2,2) geometry optimization leads to a nonplanar structure whose phenyl groups rotate out of the molecular plane.[47] In the conventional DFT method with the B3LYP functional, calculations with the 6-31G(d) and cc-pVDZ basis sets give a planar conformation for the trans isomer,[50,106] while recent computations with the 6-31G(d,p), 6-311G(d,p), and 6-311+G(2d,p) basis sets predict a nonplanar geometry.[107] The present SF-BHHLYP/DH(d,p) calculation predicts a planar conformation for the trans isomer. CCSD(T) (coupled cluster single and double excitations with perturbative triple excitations) calculations with an extrapolation to the complete basis set limit have predicted that the energy difference is 0.3 kcal/mol in favor of the planar form.[105] The cis isomer, $(S_0)_{cis}$, has an approximately C_2 geometry. The cis $\angle C_2C_1C_8$ and $\angle C_1C_8C_9$ bond angles increase by 4° with respect to the trans isomer. In addition, twisting motions are observed for the central C_1C_8 bond ($\tau = 5°$) and the phenyl groups ($\alpha = 35°, \beta = 33°$). These changes are due to the steric repulsion between the benzene rings in the cis conformation. The remaining geometrical parameters are very similar to those of the trans isomer. The optimized geometry is in good agreement with those in the gas-phase electron diffraction experiment ($\tau = 5°$ and $\alpha = 43°$).[103]

The vertical excitation energy to the S_1 state is calculated to be 4.78 and 4.45 eV for the cis and trans isomers, respectively. These values are comparable to the experimental results in *n*-hexane solution (~4.6 and ~4.1 eV), and they follow the same trends.[16] Several theoretical studies have reported the vertical excitation energies of *cis*- and *trans*-stilbene: 4.09 and 3.94 eV by the LR-TDDFT (TD-PBE0) approach,[53] 6.07 and 5.74 eV by the SA-2-CAS(2,2) method,[47] and 5.73 eV for the trans isomer with MS-CASPT2.[96] It is surprising that the excitation energy difference between the SFDFT and MS-CASPT2 methods is more than 1 eV, considering that the SF-BHHLYP "active space" is comparable to the CAS(2,2) active space. For the trans isomer, the large

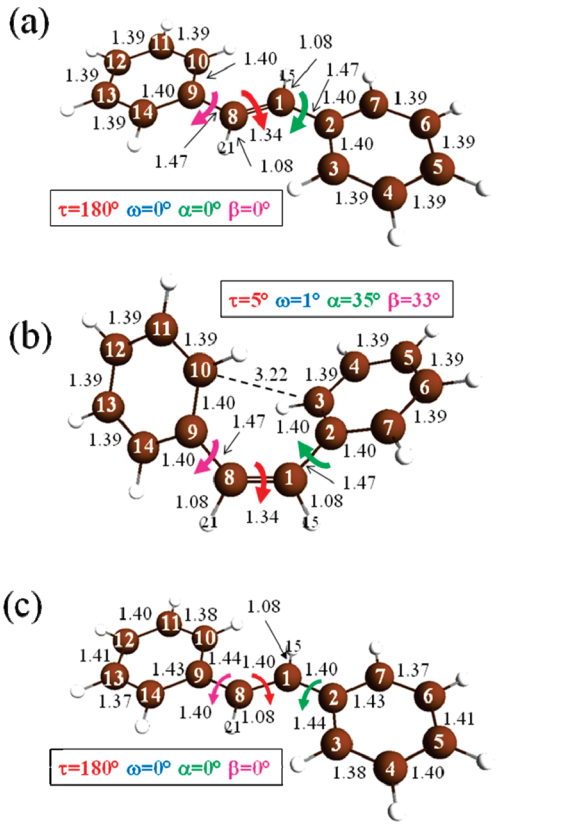

Figure 2. SF-BHHLYP optimized geometries for the ground state (a) trans and (b) cis isomers and (c) the S_1 *trans*-stilbene. Bond lengths are in angstroms, and angles are in degrees.

discrepancy may be partly attributed to the difference in the predicted ground-state optimized geometries by the two methods: the present SFDFT approach predicts a planar (C_{2h}) geometry, while the CAS(2,2) calculation finds a phenyl rotation out of the molecular plane. The previous LR-TDDFT study has pointed out that the vertical transition energy depends strongly on the degree of phenyl rotation.[51] In addition to the planarity issue, there has been a source of some controversy about the ordering of excited states for both cis and trans isomers. The correct energetic order is essential to obtain an adequate understanding of the fundamental aspects of the photoisomerization process. For the trans isomer, there are three low-lying excited singlet states: $1B_u$, $2B_u$, and $2A_g$ in the C_{2h} point group. Molina et al.[43] have applied the state-specific CASPT2 method to *trans*-stilbene and assigned the highest occupied MO (HOMO)-lowest unoccupied MO (LUMO) transition to the $2B_u$ state and the combination of HOMO to LUMO+1 and HOMO-1 to LUMO excitations to the $1B_u$ state. The HOMO ($4a_u$) and LUMO ($4b_g$) are localized on the central ethylene unit, and the HOMO-1 ($3a_u$) and LUMO+1 ($5b_g$) are described as a linear combination of MOs localized on the benzene rings. As a result, *trans*-stilbene is predicted by CASPT2 to be initially excited to the optically allowed $2B_u$ state. On the contrary, the MS-CASPT2[45] and LR-TDDFT[51−53] studies agree that the $1B_u$ state is described by the HOMO−LUMO excitation, although the excitation energies are sensitive to the active space that is chosen in the former method. Recently, Angeli et al.[54] have applied a different version of multireference perturbation theory (*n*-electron valence state perturbation theory) to *trans*-stilbene and reproduced the

energetic ordering predicted by the LR-TDDFT method: the $1B_u$ state has HOMO−LUMO character, and the resultant oscillator strength is large. For the cis isomer, state-specific CASPT2[44] calculations have assigned the HOMO−LUMO excitation to the S_3 state. Following this CASPT2 calculation, Fuss et al.[18,19] have proposed an ultrafast decay from the S_3 to the S_1 state within 25 fs that is too fast to be probed experimentally. In contrast, Improta and Santoro[53] have applied the LR-TDDFT method to compute the excitation energies of the cis isomer and found that the S_1 state is described exclusively by the HOMO −LUMO transition. Thus, according to the LR-TDDFT study, the mechanism of fast decay to the S_1 state is not necessary. Recently, Nakamura et al.[22] have measured the steady-state fluorescence of *cis*-stilbene and estimated the oscillator strength of the fluorescence to be 0.17, indicating that the S_1 state of the cis isomer is an optically allowed state. The present calculations are in agreement with the previous LR-TDDFT results for both isomers; i.e., the S_1 state is described as a HOMO−LUMO transition.

Finally, the SF-BHHLYP calculations show that in the ground electronic state the *trans*-stilbene isomer is more stable than the cis isomer by 4.7 kcal/mol. The calculated results reproduce quantitatively the enthalpy of cis to trans isomerization, +4.6 kcal/mol, measured in benzene solution at 298 K.[108] The quantitative agreement is in stark contrast with the very small energy difference (0.2 kcal/mol) computed by the state-specific CASPT2 method.[44]

3.2. Excited State Energy Minima and S_0/S_1 Conical Intersections. The present SFDFT study has located three excited state energy minima, for the S_1 state and the two CI points connecting the S_0 and S_1 states. The three SF-BHHLYP optimized geometries are presented and discussed first. The energetic information is described in the next subsections. Figure 2c shows the S_1 trans minimum geometry, $(S_1)_{trans}$. As for $(S_0)_{trans}$, $(S_1)_{trans}$ has approximately C_{2h} symmetry with $\tau = 180°$ and $\omega = 0°$, and the phenyl rings are in the molecular plane ($\alpha = 0°$ and $\beta = 0°$). The bond alternation observed for the ground-state geometry diminishes in the S_1 state due to the $\pi \rightarrow \pi^*$ excitation; the central C_1-C_8 bond length increases by 0.06 Å, while the C_1-C_2 and C_8-C_9 bonds shrink by 0.07 Å.

The PES around twisted S_1 stilbene has valuable information regarding the cis−trans isomerization mechanism. As mentioned in the Introduction, the conventional LR-TDDFT method cannot access the twisted stilbene structure.[53,55] Therefore, the present SFDFT approach can fill in a missing part of the excited-state PES for S_1 stilbene. The twisted minimum geometry (Figure 3a) has a nearly perpendicular ($\tau = 86°$) arrangement and is considerably pyramidalized ($\omega = 52°$), and thus the label $(S_1)_{pyr}$ is assigned. The prediction of the true minimum in a twisted conformation supports the prediction of a "phantom" state that has recently been identified by experiments.[18,25] Compared to the Franck−Condon (FC) geometry, $(S_0)_{trans}$, the central C_1-C_8 bond length increases by 0.08 Å, while the C_1-C_2 (C_8-C_9) vinyl−phenyl bond decreases by 0.02 (0.05) Å. A sizable dipole moment (8.01 D) is found at the twisted conformation. The dominant transition amplitude is the spin-flip excitation from the p orbital of the C_8 atom to that of the C_1 atom. A charge migration is clearly seen in the Mulliken population analysis, where the largest change is observed for the C_1 and C_8 atoms in the ethylene bond: the Mulliken charges for these atoms are −0.51 and 0.00 in the S_1 state, while the charges are nearly equal in the reference triplet state (−0.26 and −0.21). It is

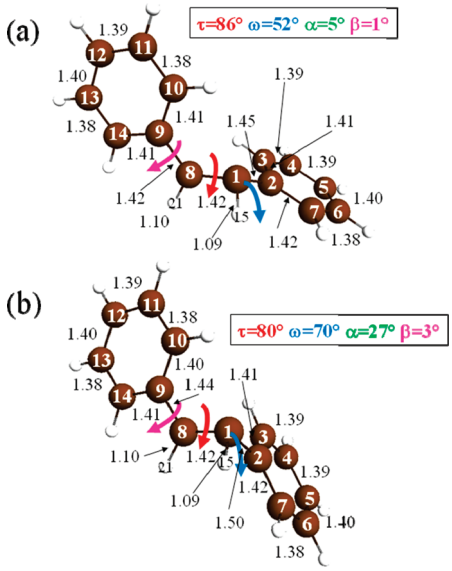

Figure 3. SF-BHHLYP optimized geometries for the twisted-pyramidalized (a) S_1 minimum and (b) S_0/S_1 conical intersection points. Bond lengths are in angstroms, and angles are in degrees.

interesting to compare the optimized geometry with that obtained by the SA-2-CAS(2,2)/6-31G method, which also finds a twisted-pyramidalized minimum ($\tau = 89°$, $\omega = 32°$).[47] A smaller pyramidalization angle at the C_1 atom implies that the SA-2-CAS(2,2) estimates a smaller charge migration than does SF-BHHLYP because the negative charge enhances the p character of the C_1 atom (cf., methyl cation vs methyl anion). Indeed, there are some differences in the optimized geometry around the C_1 atom. Although the average twisting angle τ is comparable, each of the four dihedral angles differs remarkably for the two methods: $\angle C_2C_1C_8C_9$, for example, is 115° (107°) for the SA-2-CAS(2,2) (SF-BHHLYP) method. In addition, the bond angles $\angle C_2C_1C_8$, $\angle C_2C_1H_{15}$, and $\angle C_8C_1H_{15}$ are 120° (114°), 117° (110°), and 108° (112°), respectively, and the phenyl twisting angle α is 0.4° (4.6°).

Using the penalty-constrained optimization method, the SFDFT calculations can successfully locate the twisted-pyramidalized CI point (Figure 3b), $(S_0/S_1)_{pyr}$. The SFDFT method identifies the CI point as the crossing between the zwitterionic and open-shell singlet ("dot−dot") states. The CI geometry is more twisted and pyramidalized ($\tau = 80°$, $\omega = 70°$) than $(S_1)_{pyr}$. The bond angle $\angle C_2C_1H_{15}$ decreases by 6°, while the dihedral angle $\angle H_{15}C_1C_8C_9$ ($\angle H_{15}C_1C_8H_{21}$) changes from 123° (58°) to 138° (45°). Interestingly, there are negligible changes in the C_1-H_{15} bond length and in the bond angle $\angle C_8C_1H_{15}$. Therefore, the difference in the pyramidalization angle ω between the $(S_0/S_1)_{pyr}$ and $(S_1)_{pyr}$ points is closely related to the out-of-plane motion of the H_{15} atom. The benzene ring motion also plays an important role. The vinyl−phenyl C_1-C_2 bond length increases from 1.45 to 1.50 Å, and the bond angle $\angle C_2C_1C_8$ decreases from 114° to 95°. At the same time, the phenyl ring rotates out of the plane from $\alpha = 5°$ to 27°. Notably, the CI geometry of stilbene is similar to that of ethylene obtained with the SF-BHHLYP/6-31G(d) method in the previous study ($\tau = 79°$ and $\omega = 66°$).[94] A similar trend has been observed for the SA-2-CAS(2,2) CI geometries of ethylene and stilbene.[47] Table 1 summarizes selected geometric parameters obtained by the

dx.doi.org/10.1021/jp203803a |J. Phys. Chem. A 2011, 115, 7901–7911

Table 1. Selected Geometrical Parameters for the Twisted-Pyramidalized Conical Intersection Structure[a]

	SF-BHHLYP/DH(d,p)		SA-3-CAS(2,2)[b]	MS-CASPT2[b]
	$(S_0/S_1)_{pyr}$	$(S_1)_{pyr}$	$(S_0/S_1)_{pyr}$	$(S_0/S_1)_{pyr}$
$\angle C_2C_1C_8C_9$	116	115	117	145
$\angle C_2C_1C_8H_{21}$	61	65	60	42
$\angle H_{15}C_1C_8C_9$	138	123	144	114
$\angle H_{15}C_1C_8H_{21}$	45	58	39	60
ω[c]	70	52	75	53
α[c]	27	5	26	4
β[c]	3	1	4	3
C_1-C_8	1.42	1.42	1.50	1.38
C_1-C_2	1.50	1.45	1.55	1.47
C_8-C_9	1.44	1.42	1.43	1.46
C_1-H_{15}	1.09	1.09	1.11	1.16
$\angle C_2C_1C_8$	95	114	94	127
$\angle C_2C_1H_{15}$	104	110	98	108
$\angle C_8C_1H_{15}$	107	108	103	76

[a] Bond lengths are in angstroms, and angles are in degrees. Atom numbering is given in Figure 1. $(S_0/S_1)_{pyr}$, the twisted-pyramidalized CI; $(S_1)_{pyr}$, the S_1 twisted-pyramidalized minimum. [b] SA-2-CAS(2,2)/6-31G(d,p) and MS-CASPT2/6-31G(d,p) calculations using the penalty constrained optimization method, ref 96. Note that the MS-CASPT2 method finds the S_0/S_1 CI point to be the global minimum on the S_1 PES. [c] Pyramidalization angle (ω) and twisting angles of benzene rings (α and β), see Figure 1.

present SF-BHHLYP method along with those predicted by the SA-3-CAS(2,2) and the MS-CASPT2 approaches.[96] Note that MS-CASPT2 finds the CI point to be the global minimum on the S_1 PES. The SF-BHHLYP CI geometry is closer to that of SA-3-CAS(2,2) than to that of MS-CASPT2. Assuming that the MS-CASPT2 method is a reliable benchmark, the SF-BHHLYP method underestimates the degree of hydrogen migration character for $(S_0/S_1)_{pyr}$: the C_1-H_{15} bond length and bond angle $\angle C_8C_1H_{15}$ are 1.09 Å and 107°, respectively, while the SA-3-CAS(2,2) (MS-CASPT2) calculations give 1.11 Å (1.16 Å) and 103° (76°). There are some similarities between the SF-BHHLYP S_1 minimum, $(S_1)_{pyr}$, and the MS-CASPT2 CI as shown in Table 1. However, the SF-BHHLYP S_1 PES is different from the MS-CASPT2 PES in that the former has a distinct energy minimum on the S_1 PES.

The S_1 PES around the cis isomer is examined to understand the ultrafast relaxation mechanism of *cis*-stilbene. A full geometry optimization was performed using the ground-state *cis*-stilbene geometry as the starting point. The resultant geometry is shown in Figure 4a. The geometric parameters are significantly different from those of the ground-state cis isomer: the C_3-C_{10} bond length (2.10 Å) is much shorter than that of the ground state cis isomer (3.22 Å), and the H_{16} and H_{22} atoms bend out of the benzene ring plane by ~30°. These structural changes indicate a partial bond formation between the C_3 and C_{10} atoms. The Meyer bond order (~0.5) suggests sizable bonding character, while no C_3-C_{10} bond formation is found (bond order < 0.05) for the ground state cis isomer. The authors of the previous LR-TDDFT study[53] pointed out that the optimization of the S_1 cis isomer leads to the cyclization product (4a,4b-dihydrophenanthrene: DHP). The TDDFT B3LYP/DH(d,p) optimized geometry (not shown) is similar to the SF-BHHLYP geometry

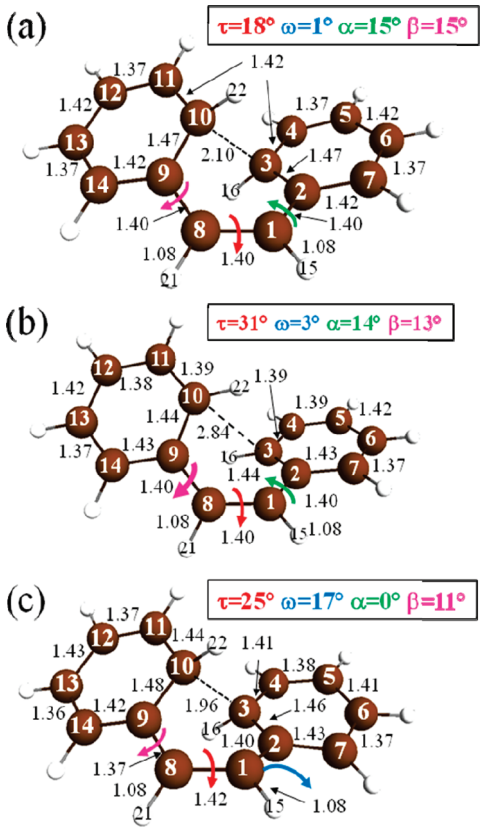

Figure 4. SF-BHHLYP geometries for (a) S_1 DHP, (b) S_1 *cis*-stilbene, and (c) S_0/S_1 cooperating-ring conical intersection. Bond lengths are in angstroms, and angles are in degrees. Note that the structure (b) is approximate due to the constrained optimization, while (a) and (c) are fully optimized.

obtained in the present work. Therefore, the fully optimized geometry shown in Figure 4a is assigned to the S_1 DHP minimum, $(S_1)_{DHP}$. Although the present study does not identify any other true minimum for the cis isomer, the experimental study on *cis*-stilbene in argon clusters[39] has observed an S_1 local minimum in the cis region. Furthermore, the semiempirical[37] and configuration interaction singles (CIS)[58,59] methods have identified a cis minimum. It is not surprising that dynamic correlation stabilizes the DHP minimum with respect to the cis minimum and/or lowers the barrier of DHP formation on the S_1 PES. In the previous LR-TDDFT study, Improta and Santoro[53] have optimized the geometries for the S_1 *cis*-stilbene by imposing the constraint that phenyl hydrogen atoms are coplanar to the benzene rings and suggested that the optimized geometry corresponds to a real minimum or, at least, to a metastable species. By adopting a similar approach, an approximate cis minimum geometry (see Figure 4b), $(S_1)_{cis}$, is obtained under the constraint that the H_{16} and H_{22} atoms are kept coplanar to the benzene rings. The $(S_1)_{cis}$ has a twisting angle (τ) of 31°, which is in good agreement with the model calculations by Todd et al.[33] (37°) and the semiempirical calculation by Warshel[37] (35°).

Another CI structure (Figure 4c) is identified at (τ,ω) = (25°,17°) using the penalty-constrained optimization method. Compared to $(S_1)_{DHP}$, the C_1-C_8 bond length and the twisting angle τ increase by 0.02 Å and 7°, respectively, while the C_8-C_9 bond shrinks by 0.03 Å. In addition, the benzene ring attached to the C_1 atom rotates from α = 15° to 0°. These structural changes

Table 2. Selected Geometrical Parameters for the Cooperating-Ring Conical Intersection Structure[a]

	SF-BHHLYP[b]	SA-3-CAS(2,2)[b,c]	SA-3-CAS(14,12)[b,c]	MMVB[d]
C_1-C_8	1.42	1.40	1.40	1.38
C_1-C_2	1.40	1.41	1.42	1.43
C_2-C_3	1.46	1.45	1.43	1.50
C_8-C_9	1.37	1.38	1.38	1.43
C_9-C_{10}	1.48	1.48	1.46	1.50
C_3-C_{10}	1.96	1.96	1.95	2.01
$\angle C_2C_1C_8$	119	119	119	108
$\angle C_1C_2C_3$	123	124	125	114
$\angle C_1C_8C_9$	122	124	123	108
$\angle C_8C_9C_{10}$	115	115	113	114
$\angle C_2C_1C_8C_9$	33	30	31	25
$\angle C_8C_1C_2C_3$	11	8	17	22
$\angle C_1C_8C_9C_{10}$	9	10	13	22

[a] Bond lengths are in angstroms, and angles are in degrees. Atom numbering is given in Figure 1. [b] This work. The DH(d,p) basis set was employed. [c] Conical intersection is optimized using the analytical gradient and derivative coupling vectors, not the penalty-constrained method. [d] Molecular mechanics valence bond calculation, ref 42.

enhance the bonding character between the C_3 and C_{10} atoms, resulting in a shorter C_3-C_{10} bond length of 1.96 Å. Bearpark et al.[42] have explored the S_1 PES of *cis*-stilbene by the molecular mechanics valence bond (MMVB) approach and successfully identified several low-lying CI points. The lowest energy CI point located by the MMVB method, the cooperating-ring CI ("X_{coop}" in ref 42), lies along the cyclization reaction coordinate to DHP rather than the cis-to-trans isomerization coordinate. Table 2 summarizes selected geometric parameters. For comparison, Table 2 also includes the SA-3-CAS(2,2)/DH(d,p) and SA-3-CAS(14,12)/DH(d,p) CI geometries optimized with the analytic gradient and derivative coupling vectors in the MOLPRO package.[109] The SF-BHHLYP CI geometry is in good agreement with the SA-3-CAS geometries, and these CI geometries determined by the ab initio methods are qualitatively similar to the MMVB result. Therefore, the identified CI geometry is the cooperating-ring CI obtained by the MMVB calculation, and the label $(S_0/S_1)_{coop}$ is assigned.

3.3. Trans-to-Cis Isomerization. Figure 5 shows the two-dimensional PES along the twisting (τ) and pyramidalization (ω) angles. At each (τ, ω) point, geometric parameters other than τ and ω are optimized. Some relevant points are also included in Figure 5 because the geometry optimization without any constraint may be thought of as the lowest energy point at the optimal τ and ω. Figure 6 summarizes the energetic information that is relevant to the isomerization reaction. The initial point just after the vertical excitation of the trans isomer, i.e., the FC point, corresponds to (τ,ω) = (180°,0°). The $(S_1)_{trans}$ structure also has (τ,ω) = (180°,0°), although the other geometrical parameters are different from those of $(S_0)_{trans}$. The $(S_1)_{trans}$ point is lower in energy by 0.39 eV than the FC point. The 0−0 adiabatic excitation energy from the $(S_0)_{trans}$ to $(S_1)_{trans}$ is computed to be 4.01 eV, which is comparable to the experimental value of 4.00 eV,[4,5,104] in vacuum, while the LR-TDDFT (B3LYP/TZVP) and SA-2-CAS(2,2)/6-31G methods predict 3.62 and 5.18 eV, respectively.[55] The emission from the $(S_1)_{trans}$ structure is one of the possible decay mechanisms. The SF-BHHLYP calculations

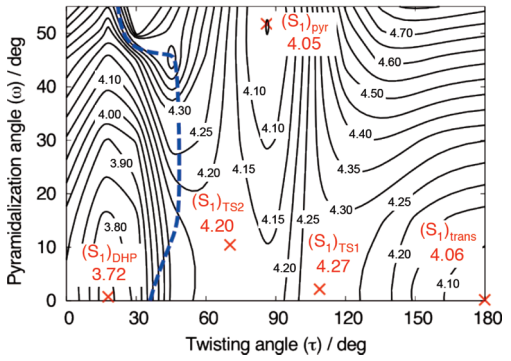

Figure 5. Two-dimensional S_1 state potential energy surface along the twisting (τ) and pyramidalization (ω) angles. At each (τ, ω) point, the remaining geometric parameters are optimized. Energy (in eV) is measured from the ground state trans minimum (180° twisting and 0° pyramidalization), and contour spacing is 0.05 eV. Several important points are shown: the trans minimum, $(S_1)_{trans}$; the twisted-pyramidalized minimum, $(S_1)_{pyr}$; the DHP (cyclization product) minimum, $(S_1)_{DHP}$; the transition states, $(S_1)_{TS1}$ and $(S_1)_{TS2}$. The blue dashed line, which connects the geometries with a 25° out-of-plane angle for the H_{16} atom, defines the boundary between the cyclization product, DHP (left), and stilbene (right). Note that the minimum energy point found at the left of the blue line corresponds to the DHP minimum.

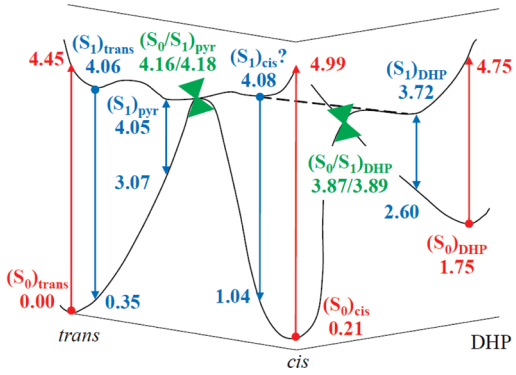

Figure 6. Schematic drawing of the potential energy surfaces for the photoisomerization reaction of stilbene. Several important points are shown: the trans minimum, $(S_0)_{trans}$ and $(S_1)_{trans}$; the cis minimum, $(S_0)_{cis}$ and $(S_1)_{cis}$; the DHP (cyclization product) minimum, $(S_0)_{DHP}$ and $(S_1)_{DHP}$; the twisted-pyramidalized minimum (phantom state), $(S_1)_{pyr}$; the twisted-pyramidalized conical intersection, $(S_0/S_1)_{pyr}$; the cooperating-ring conical intersection, $(S_0/S_1)_{coop}$. Note that the $(S_1)_{cis}$ is not a true minimum due to the constrained optimization. The energy (in eV) is measured from the ground-state trans minimum (180° twisting and 0° pyramidalization).

give a fluorescence energy of 3.71 eV, which is in good agreement with the experimental fluorescence maximum of 3.71 eV in *n*-hexane solution.[110]

Now, consider the trans-to-cis isomerization reaction. The trans-to-cis isomerization proceeds very slowly (10−200 ps),[9,10,24,25,36] and such a slow process is attributed to a large barrier along the reaction coordinate. The barrier height has been estimated to be ~3.3 kcal/mol by experiment[3,4,6,32] and recently computed to be 2.1 kcal/mol (3.9 kcal/mol before the ZPE correction)[48] by adding the CASPT2 PT2 correlation energy with a SA-2-CAS(2,2) reference to the SA-5-CAS(14,12) energy. The transition state optimized by the SF-BHHLYP method in

dx.doi.org/10.1021/jp203803a |J. Phys. Chem. A 2011, 115, 7901–7911

this work, $(S_1)_{TS1}$, is found at $(\tau, \omega) = (109°, 2°)$, and the barrier height is calculated to be 3.4 kcal/mol (0.15 eV) [4.8 kcal/mol (0.21 eV) before the ZPE correction] with respect to the $(S_1)_{trans}$. The $(S_1)_{TS1}$ geometry is given in the Supporting Information. Therefore, the present SFDFT value is close to the experimental estimate. However, the reactive frequency is calculated to be $41i$ cm^{-1}, much smaller than the $607i$ cm^{-1} obtained by the SA-2-CAS(2,2) method.[48] While the experiment[10] has predicted that the barrier frequency must be greater than 160 cm^{-1}, Schroeder et al.[49] have chosen the 25 cm^{-1} mode obtained by the CIS method to be the reaction coordinate and fitted the rate constant by adjusting the barrier height. The optimal barrier height is in reasonable agreement with the experimental threshold value, in spite of the small imaginary frequency. Finally, consider the nonadiabatic effects on the barrier formation. Orlandi and Siebrand[111] have considered the two interacting benzyl radicals to interpret the isomerization barrier of stilbene; thus, the model consists of four electronic states like the N, V, Z, and T states in ethylene. According to this model, the S_1 barrier formation is attributed to the crossing between the S_1 and S_2 (V and Z) states. Negri and Orlandi[112] have optimized the transition state using semiempirical configuration interaction calculations with and without the doubly excited configurations to estimate the mixing of the 1B (V) and 2A (Z) states. The calculated rate constant shows that the avoided crossing of these two states is the main reason for the transition state formation. On the contrary, the present SF-BHHLYP calculations show no evidence for the participation of the 2A state; the doubly excited (Z) state is higher in energy than that of the V state by 0.39 eV. Furthermore, the S_1 state involves a negligible (<0.05) transition amplitude for the double excitation, i.e., from π_α to π_β^* with respect to the $\pi_\alpha\pi_\alpha^*$ reference triplet state. Therefore, nonadiabatic effects are expected to be marginal at the identified transition state. Interestingly, Molina et al.[43] have proposed another mechanism in which the isomerization barrier is produced by the interaction of the 1B and 2B states along the twisting coordinate.

After crossing the barrier, *trans*-stilbene leads to the perpendicular conformation, where the PES is relatively flat along the pyramidalization coordinate. Therefore, some molecules increase the pyramidalization angle and reach the twisted minimum, $(S_1)_{pyr}$, and the others continue to twist further toward the cis isomer adiabatically on the S_1 state PES. A dynamics simulation is necessary to estimate the branching ratio. First, consider the former process. The twisted-pyramidalized minimum, $(S_1)_{pyr}$, is located at $(\tau,\omega) = (86°,52°)$ and is nearly isoenergetic with $(S_1)_{trans}$, while the previous SA-2-CAS(2,2) study[47] has predicted a large stabilization (0.59 eV) by the C=C twisting motion. The $(S_1)_{pyr}$ energy is 0.13 eV larger than that of the purely twisted geometry which is optimized with the constraint of $(\tau,\omega) = (90°,0°)$. This indicates that the nonpyramidalized structure is not a minimum on the S_1 potential energy surface. In contrast, the MMVB study by Bearpark et al.[42] identified a planar perpendicular minimum ("M_{perp}" in ref 42), which may be attributed to the fact that the MMVB method does not include ionic states. In the present SFDFT calculations, the S_1 state is ionic around the twisted conformation even without the pyramidalization. At the $(S_1)_{pyr}$ point, the SF-BHHLYP energy gap between the S_0 and S_1 states is estimated to be 0.98 eV, and a rapid internal conversion is unlikely to take place. Such a large energy gap is in contrast to ethylene, in which the global S_1 minimum leads to the CI. The CI point, $(S_0/S_1)_{pyr}$, is located at $(\tau,\omega) = (80°,70°)$ and is higher in energy by 0.13 eV than the $(S_1)_{pyr}$ minimum. The SA-2-CAS(2,2) study[47] predicted that the energy difference between the $(S_1)_{pyr}$ and $(S_0/S_1)_{pyr}$ points is 0.46 eV; the large energy difference is partly due to the lack of dynamic correlation effects. The authors of the recent MS-CASPT2 study[96] have pointed out that the optimization of the $(S_0/S_1)_{pyr}$ CI point leads to the absolute minimum on the S_1 PES. When stilbene approaches the $(S_0/S_1)_{pyr}$ point, the molecule returns to the ground state easily by efficient internal conversion. On the vibrationally hot ground state, some molecules complete the twisting motion and lead to the cis isomer (product), and the others go back to the initial trans isomer (reactant).

Next, consider the case in which the photoexcited stilbene continues to twist toward the cis isomer adiabatically on the S_1 PES. A second barrier, $(S_1)_{TS2}$, is found at $(\tau,\omega) = (71°,10°)$. The $(S_1)_{TS2}$ geometry is given in the Supporting Information. The barrier height is estimated to be 1.6 kcal/mol (0.07 eV) [3.3 kcal/mol (0.14 eV) before the ZPE correction] with respect to the $(S_1)_{trans}$ structure. The molecule can surmount this barrier easily because the second barrier height is smaller than the first by 1.8 kcal/mol. After crossing the barrier, the molecule approaches the cis region on the S_1 PES. The SF-BHHLYP calculations, however, predict that the cyclization product, DHP, is more stable than *cis*-stilbene. In Figure 5, the "boundary" between *cis*-stilbene and DHP is tentatively defined as the dashed line corresponding to the geometries with a 25° out-of-plane angle for the H_{16} atom because this angle changes drastically from ~0 to 30° in crossing the boundary. There are three important points, $(S_1)_{cis}$, $(S_1)_{DHP}$, and $(S_0/S_1)_{coop}$, located at $(\tau,\omega) = (31°,3°)$, $(18°,1°)$, and $(25°,17°)$, respectively. The fluorescence decay from the cis minimum is a possible relaxation mechanism. Although $(S_1)_{cis}$ is an approximate minimum, the calculated emission energy of 3.05 eV is in good agreement with the experimental value of ~3 eV in cyclohexane[22] and *n*-hexane[30] solutions. $(S_1)_{DHP}$ is the true minimum energy point on the S_1 PES and is exothermic by 0.3−0.4 eV with respect to $(S_1)_{cis}$, $(S_1)_{pyr}$, and $(S_1)_{trans}$. The unconstrained geometry optimization started at the $(S_1)_{cis}$ point leads to $(S_1)_{DHP}$, implying that $(S_1)_{cis}$ is a potential intermediate in the DHP formation reaction. Although the barrier on the DHP path is not identified in the present work, experiments have estimated the barrier height to be 2.0 and 1.2 kcal/mol.[17,113] The SF-BHHLYP emission energy at the $(S_1)_{DHP}$ point is calculated to be 1.12 eV, which is at variance with the experimental fluorescence energy (~3 eV) expected to be from the cis minimum. In addition, a very weak DHP emission[1,24,25] indicates that the fluorescence decay is an inefficient mechanism. The radiationless decay is also suppressed at the DHP minimum due to the relatively large energy gap (1.12 eV). Therefore, the $(S_0/S_1)_{coop}$ CI point is the most likely candidate to account for the rapid relaxation around the DHP minimum because of the slight endothermicity (0.17 eV) with respect to $(S_1)_{DHP}$. Jiang et al.[63] have performed a molecular dynamics simulation and found that DHP is formed from the *trans*-stilbene reactant through the excited *cis*-stilbene intermediate. The present SF-BHHLYP calculations support the direct DHP formation from *trans*-stilbene on the S_1 state PES.

3.4. Cis-to-Trans Isomerization. The cis-to-trans isomerization proceeds much more easily than the trans-to-cis isomerization. Experimental results indicate a negligibly small barrier along the isomerization path.[17,24,25,27,30,34] The SF-BHHLYP calculations support the reaction from cis to the perpendicular conformation. The FC point for the cis isomer is at $(\tau,\omega) = (5°,1°)$

and is 0.54 eV higher in energy than the trans FC point. Thus, the photoexcited stilbene has a larger excess energy in the cis-to-trans isomerization than in the trans-to-cis reaction. Using the approximate minimum, $(S_1)_{cis}$, the barrier height at $(S_1)_{TS2}$ is estimated to be 0.12 eV without the ZPE correction. A smaller barrier along the cis-to-trans reaction is consistent with the shorter *cis*-stilbene lifetime observed in the experiments. In the perpendicular conformation, some molecules reach the $(S_0/S_1)_{pyr}$ CI point through $(S_1)_{pyr}$, and the others continue to twist toward the trans isomer adiabatically on the S_1 PES. The former process is similar to that in the *trans*-stilbene isomerization discussed above, but the cis isomer reaction is expected to be much easier than the trans isomer because of the larger excess energy. The same relaxation mechanism, i.e., the rapid internal conversion through the $(S_0/S_1)_{pyr}$ CI point, could explain the experimental observation that the product yield is independent of whether the initial reactant is the cis or trans isomer. To examine the possibility of the adiabatic cis-to-trans reaction on the S_1 PES, Saltiel et al.[29,30] have measured the fluorescence of *cis*-stilbene by removing carefully the *trans*-stilbene and concluded that the excited trans isomer is formed from the cis isomer adiabatically on the S_1 PES. The present calculations support the adiabatic reaction because the barrier height at $(S_1)_{TS1}$ is almost the same for both the cis-to-trans and trans-to-cis directions.

In the *cis*-stilbene photochemistry, the cyclization product, DHP, is formed in addition to the trans isomerization product. There are three points relevant to the relaxation of S_1 *cis*-stilbene: $(S_1)_{DHP}$, $(S_0/S_1)_{coop}$, and $(S_1)_{cis}$ located at (18°,1°), (25°,17°), and (31°,3°), respectively. The SF-BHHLYP optimized geometries indicate that the twisting angles of the phenyl groups (α and β) also play an important role to reach these points (Figure 4). From the FC point at (5°,1°), the excited *cis*-stilbene relaxes toward one of these points. If the twisting motion around the central ethylene bond is dominant at the FC point, the molecule reaches the $(S_1)_{cis}$ approximate minimum followed by $(S_1)_{DHP}$ or $(S_1)_{pyr}$. The first step involves the twisting motion (τ) by 26° and the phenyl twisting motions (α and β) by −21° and −20°. The reaction channel for DHP formation is open for the $(S_1)_{cis}$ structure because the unconstrained geometry optimization of $(S_1)_{cis}$ leads to $(S_1)_{DHP}$. Thus, the product yield of DHP and *trans*-stilbene depends on the branching ratio at the $(S_1)_{cis}$ point. Since $(S_1)_{DHP}$ has a small oscillator strength and there is a large energy gap (1.12 eV) between the S_0 and S_1 states, there must be another decay channel to account for the efficient relaxation of *cis*-stilbene. $(S_0/S_1)_{coop}$ is one of the possible pathways connecting the S_0 and S_1 states. It is easy to reach the $(S_0/S_1)_{coop}$ CI point from $(S_1)_{DHP}$ because the former is only slightly higher in energy (0.17 eV) than the latter. Sufficient kinetic energy is available for $(S_1)_{DHP}$ due to the large energy difference between $(S_1)_{DHP}$ and the cis FC point (1.27 eV). If the reaction coordinate around the FC point includes both the pyramidalization angle (ω) and the phenyl ring twisting angles (α and β), the direct approach from the FC point to the $(S_0/S_1)_{coop}$ CI may be possible. In this case, it is necessary for the geometry to change the angles ω, α, and β by +16°, −35°, and −22°, respectively. Therefore, the initial motion (torsion or pyramidalization) at the FC point is a critical factor to account for the product yield.

Several points are unresolved in the present analysis of the PES. First, it is necessary to examine whether or not the cis minimum is formed in the excited state. Molecular dynamics simulations would be useful to confirm the metastable species and to examine how long it takes to escape from the local minimum if the molecule is kinetically trapped. In addition, the present analysis cannot account for the product yield. The experimental product yield observed for *cis*-stilbene consists of the cis−trans isomerization (35%), the formation of DHP (10%), and the recovery of reactants (55%).[40,66] However, the SF-BHHLYP method predicts that $(S_0/S_1)_{coop}$ is more stable than the $(S_0/S_1)_{pyr}$ structure by 0.28 eV and that the former channel would be dominant from the thermodynamic point of view. This discrepancy implies that the reaction of *cis*-stilbene is kinetically controlled. The first possibility is that both the $(S_0/S_1)_{coop}$ and $(S_0/S_1)_{pyr}$ CI points are operative but that the reaction path toward the former is suppressed for some reason. Here, the suppressed path means the $(S_1)_{cis}$ to $(S_1)_{DHP}$ process or the direct approach to $(S_0/S_1)_{coop}$ from the FC point. On the basis of resonance Raman spectra, Myers and Mathies[28] have discussed the initial motion of *cis*-stilbene on the S_1 state and shown that the wavepacket motion on the excited state produces a 25° torsion around the central ethylenic bond in only 20 fs. Thus, a majority of the *cis*-stilbene molecules approach the twisted-pyramidalized CI point, $(S_0/S_1)_{pyr}$, which leads to the ground state cis and trans isomers. The second possibility is that the $(S_0/S_1)_{pyr}$ formation path is closed in the photochemistry of *cis*-stilbene. Rather, it could be the ground state PES near the $(S_0/S_1)_{coop}$ CI point that determines the product yield. On the basis of the experiments of *cis*-stilbene homologue molecules, Petek et al.[40] have suggested that the initial direction of geometry relaxation on the S_1 state is along the photocyclization reaction coordinate rather than the cis-to-trans isomerization coordinate. Another possibility is that *cis*-stilbene approaches both the $(S_0/S_1)_{coop}$ and $(S_0/S_1)_{pyr}$ CI points. Dou and Allen[61] have performed direct dynamics simulations for *cis*-stilbene on the S_1 state by using Hamiltonian matrix elements fitted to tight-binding local-density approximation DFT calculations. The authors found two principal avoided crossings along the single trajectory and proposed that the first crossing point leads to DHP formation and the second to the *trans*-stilbene product. In this mechanism, the product yield depends on the switching probability, or the nonadiabatic coupling, at these points. It would be interesting to employ SFDFT nonadiabatic dynamics simulations to provide insight into the photochemical processes of *cis*-stilbene.

4. CONCLUSIONS

The present study has applied the SFDFT method to examine the photoisomerization of stilbene. The SF-BHHLYP method can successfully locate not only the excited-state minimum energy points but also two conical intersections, $(S_0/S_1)_{pyr}$ and $(S_0/S_1)_{coop}$. The former is similar to the twisted-pyramidalized ethylene observed in the previous study, and the latter possibly lies on the cyclization product (DHP) formation pathway. The SFDFT method locates a distinct twisted-pyramidalized minimum that is lower in energy by 0.13 eV than the $(S_0/S_1)_{pyr}$ CI point. Therefore, the present SFDFT calculations support the phantom state that has recently been identified by experiments, although the recent MS-CASPT2 study has shown that the $(S_0/S_1)_{pyr}$ point is a global minimum of the excited-state PES like the ethylene molecule. The SF-BHHLYP calculations have predicted that the S_1 state is ionic around the perpendicular conformation and that the purely twisted nonpyramidalized structure is not a true minimum for the S_1 state. To elucidate the mechanism of cis−trans isomerization, the two-dimensional PES has been

constructed as a function of the twisting and pyramidalization angles. In the trans-to-cis route, the SF-BHHLYP method locates a barrier of 3.4 kcal/mol along the isomerization path, supporting a surprisingly long lifetime for *trans*-stilbene. In addition to the nonadiabatic process through the $(S_0/S_1)_{pyr}$ CI point, the adiabatic DHP formation from *trans*-stilbene on the S_1 surface has been shown to be possible. For the cis-to-trans reaction, some possible decay mechanisms have been proposed: radiationless decay through $(S_0/S_1)_{pyr}$ and DHP formation through $(S_0/S_1)_{coop}$.

In the present study, the isomerization mechanisms of stilbene are discussed on the basis of the excited state PES only. As a result, the information of some quantities that are relevant to the excited-state dynamics is still missing. To explain the lifetime and product yield, it is necessary to perform nonadiabatic dynamics simulations to monitor the relaxation processes and product formation on the fly. There have been several papers on the calculation of the nonadiabatic coupling matrix element within the linear-response TDDFT, and the extension to the SFDFT method is straightforward. Work is in progress along these lines.

■ ASSOCIATED CONTENT

Supporting Information. Cartesian coordinates for all geometries discussed in the text and energies for relevant electronic states. This material is available free of charge via the Internet at http://pubs.acs.org.

■ AUTHOR INFORMATION

Corresponding Author
*E-mail: mark@si.msg.chem.iastate.edu.

■ ACKNOWLEDGMENT

This work was supported by grants from the Air Force Office of Scientific Research and a National Science Foundation Petascale Applications grant.

■ REFERENCES

(1) Waldeck, D. H. *Chem. Rev.* **1991**, *91*, 415–436.
(2) Görner, H.; Kuhn, H. J. *Adv. Photochem.* **1995**, *19*, 1–117.
(3) Syage, J. A.; Lambert, W. R.; Felker, P. M.; Zewail, A. H.; Hochstrasser, R. M. *Chem. Phys. Lett.* **1982**, *88*, 266–270.
(4) Syage, J. A.; Felker, P. M.; Zewail, A. H. *J. Chem. Phys.* **1984**, *81*, 4685–4705.
(5) Syage, J. A.; Felker, P. M.; Zewail, A. H. *J. Chem. Phys.* **1984**, *81*, 4706–4723.
(6) Felker, P. M.; Zewail, A. H. *J. Phys. Chem.* **1985**, *89*, 5402–5411.
(7) Pedersen, S.; Bañares, L.; Zewail, A. H. *J. Chem. Phys.* **1992**, *97*, 8801–8804.
(8) Baumert, T.; Frohnmeyer, T.; Kiefer, B.; Niklaus, P.; Strehle, M.; Gerber, G.; Zewail, A. H. *Appl. Phys. B: Laser Opt.* **2001**, *72*, 105–108.
(9) Rothenberger, G.; Negus, D. K.; Hochstrasser, R. M. *J. Chem. Phys.* **1983**, *79*, 5360–5367.
(10) Lee, M.; Holtom, G. R.; Hochstrasser, R. M. *Chem. Phys. Lett.* **1985**, *118*, 359–363.
(11) Abrash, S.; Repinec, S. T.; Hochstrasser, R. M. *J. Chem. Phys.* **1990**, *93*, 1041–1053.
(12) Sension, R. J.; Repinec, S. T.; Hochstrasser, R. M. *J. Phys. Chem.* **1991**, *95*, 2946–2948.
(13) Repinec, S. T.; Sension, R. J.; Szarka, A. Z.; Hochstrasser, R. M. *J. Phys. Chem.* **1991**, *95*, 10380–10385.
(14) Sension, R. J.; Szarka, A. Z.; Hochstrasser, R. M. *J. Chem. Phys.* **1992**, *97*, 5239–5242.
(15) Sension, R. J.; Repinec, S. T.; Szarka, A. Z.; Hochstrasser, R. M. *J. Chem. Phys.* **1993**, *98*, 6291–6315.
(16) Rice, J. K.; Baronavski, A. P. *J. Phys. Chem.* **1992**, *96*, 3359–3366.
(17) Nikowa, L.; Schwarzer, D.; Troe, J.; Schroeder, J. *J. Chem. Phys.* **1992**, *97*, 4827–4835.
(18) Fuss, W.; Kosmidis, C.; Schmid, W. E.; Trushin, S. A. *Chem. Phys. Lett.* **2004**, *385*, 423–430.
(19) Fuss, W.; Kosmidis, C.; Schmid, W. E.; Trushin, S. A. *Angew. Chem., Int. Ed.* **2004**, *43*, 4178–4182.
(20) Ishii, K.; Takeuchi, S.; Tahara, T. *Chem. Phys. Lett.* **2004**, *398* 400–406.
(21) Ishii, K.; Takeuchi, S.; Tahara, T. *J. Phys. Chem. A* **2008**, *112* 2219–2227.
(22) Nakamura, T.; Takeuchi, S.; Suzuki, N.; Tahara, T. *Chem. Phys. Lett.* **2008**, *465*, 212–215.
(23) Takeuchi, S.; Ruhman, S.; Tsuneda, T.; Chiba, M.; Taketsugu, T.; Tahara, T. *Science* **2008**, *322*, 1073–1077.
(24) Sajadi, M.; Dobryakov, A. L.; Garbin, E.; Ernsting, N. P.; Kovalenko, S. A. *Chem. Phys. Lett.* **2010**, *489*, 44–47.
(25) Kovalenko, S. A.; Dobryakov, A. L.; Ioffe, I.; Ernsting, N. P. *Chem. Phys. Lett.* **2010**, *493*, 255–258.
(26) Weigel, A.; Ernsting, N. P. *J. Phys. Chem. B* **2010**, *114*, 7879–7893.
(27) Greene, B. I.; Farrow, R. C. *J. Chem. Phys.* **1983**, *78*, 3336–3338.
(28) Myers, A. B.; Mathies, R. A. *J. Chem. Phys.* **1984**, *81*, 1552–1558.
(29) Saltiel, J.; Waller, A. S.; Sun, Y.-P.; Sears, D. F., Jr. *J. Am. Chem. Soc.* **1990**, *112*, 4580–4581.
(30) Saltiel, J.; Waller, A. S.; Sears, D. F., Jr. *J. Am. Chem. Soc.* **1993**, *115*, 2453–2465.
(31) Courtney, S. H.; Fleming, G. R. *J. Chem. Phys.* **1985**, *83*, 215–222.
(32) Todd, D. C.; Jean, J. M.; Rosenthal, S. J.; Ruggiero, A. J.; Yang, D.; Fleming, G. R. *J. Chem. Phys.* **1990**, *93*, 8658–8668.
(33) Todd, D. C.; Fleming, G. R.; Jean, J. M. *J. Chem. Phys.* **1992**, *97*, 8915–8925.
(34) Todd, D. C.; Fleming, G. R. *J. Chem. Phys.* **1993**, *98*, 269–279.
(35) Bao, J.; Weber, P. M. *J. Phys. Chem. Lett.* **2010**, *1*, 224–227.
(36) Briney, K. A.; Herman, L.; Boucher, D. S.; Dunkelberger, A. D.; Crim, F. F. *J. Phys. Chem. A* **2010**, *114*, 9788–9794.
(37) Warshel, A. *J. Chem. Phys.* **1975**, *62*, 214–221.
(38) Troe, J.; Weitzel, K.-M. *J. Chem. Phys.* **1988**, *88*, 7030–7039.
(39) Petek, H.; Fujiwara, Y.; Kim, D.; Yoshihara, K. *J. Am. Chem. Soc.* **1988**, *110*, 6269–6270.
(40) Petek, H.; Yoshihara, K.; Fujiwara, Y.; Lin, Z.; Penn, J. H.; Frederick, J. H. *J. Phys. Chem.* **1990**, *94*, 7539–7543.
(41) Frederick, J. H.; Fujiwara, Y.; Penn, J. H.; Yoshihara, K.; Petek, H. *J. Phys. Chem.* **1991**, *95*, 2845–2858.
(42) Bearpark, M. J.; Bernardi, F.; Clifford, S.; Olivucci, M.; Robb, M. A.; Vreven, T. *J. Phys. Chem. A* **1997**, *101*, 3841–3847.
(43) Molina, V.; Merchán, M.; Roos, B. O. *J. Phys. Chem. A* **1997**, *101*, 3478–3487.
(44) Molina, V.; Merchán, M.; Roos, B. O. *Spectrochim. Acta, Part A* **1999**, *55*, 433–446.
(45) Gagliardi, L.; Orlandi, G.; Molina, V.; Malmqvist, P.-Å.; Roos, B. O. *J. Phys. Chem. A* **2002**, *106*, 7355–7361.
(46) Amatatsu, Y. *Chem. Phys. Lett.* **1999**, *314*, 364–368.
(47) Quenneville, J.; Martínez, T. J. *J. Phys. Chem. A* **2003**, *107*, 829–837.
(48) Leitner, D. M.; Levine, B.; Quenneville, J.; Martínez, T. J.; Wolynes, P. G. *J. Phys. Chem. A* **2003**, *107*, 10706–10716.
(49) Schroeder, J.; Steinel, T.; Troe, J. *J. Phys. Chem. A* **2002**, *106*, 5510–5516.
(50) Kwasniewski, S. P.; Deleuze, M. S.; François, J. P. *Int. J. Quantum Chem.* **2000**, *80*, 672–680.
(51) Improta, R.; Santoro, F.; Dietl, C.; Papastathopoulos, E.; Gerber, G. *Chem. Phys. Lett.* **2004**, *387*, 509–516.
(52) Dietl, C.; Papastathopoulos, E.; Niklaus, P.; Improtra, R.; Santoro, F.; Gerber, G. *Chem. Phys.* **2005**, *310*, 201–211.
(53) Improta, R.; Santoro, F. *J. Phys. Chem. A* **2005**, *109*, 10058–10067.

(54) Angeli, C.; Improta, R.; Santoro, F. *J. Chem. Phys.* **2009**, *130*, 174307−1–174307−6.
(55) Tatchen, J.; Pollak, E. *J. Chem. Phys.* **2008**, *128*, 164303−1–164303−15.
(56) Vachev, V. D.; Frederick, J. H.; Grishanin, B. A.; Zadkov, V. N.; Koroteev, N. I. *Chem. Phys. Lett.* **1993**, *215*, 306–314.
(57) Vachev, V. D.; Frederick, J. H.; Grishanin, B. A.; Zadkov, V. N.; Koroteev, N. I. *J. Phys. Chem.* **1995**, *99*, 5247–5263.
(58) Berweger, C. D.; van Gunsteren, W. F.; Müller-Plathe, F. *J. Chem. Phys.* **1998**, *108*, 8773–8781.
(59) Berweger, C. D.; van Gunsteren, W. F.; Müller-Plathe, F. *J. Chem. Phys.* **1999**, *111*, 8987–8999.
(60) Dou, Y.; Allen, R. E. *Chem. Phys. Lett.* **2003**, *378*, 323–329.
(61) Dou, Y.; Allen, R. E. *J. Chem. Phys.* **2003**, *119*, 10658–10666.
(62) Jiang, C.-W.; Xie, R.-H.; Li, F.-L.; Allen, R. E. *Chem. Phys. Lett.* **2009**, *474*, 263–267.
(63) Jiang, C.-W.; Xie, R.-H.; Li, F.-L.; Allen, R. E. *Chem. Phys. Lett.* **2010**, *487*, 177–182.
(64) Debnarova, A.; Techert, S.; Schmatz, S. *J. Chem. Phys.* **2006**, *125*, 224101−1–224101−9.
(65) Tranca, D. C.; Neufeld, A. A. *J. Chem. Phys.* **2010**, *132*, 134109−1–134109−9.
(66) Bernardi, F.; Olivucci, M.; Robb, M. A. *Chem. Soc. Rev.* **1996**, *25*, 321–328.
(67) Levine, B. G.; Martínez, T. J. *Annu. Rev. Phys. Chem.* **2007**, *58*, 613–634.
(68) Virshup, A. M.; Punwong, C.; Pogorelov, T. V.; Lindquist, B. A.; Ko, C.; Martínez, T. J. *J. Phys. Chem. B* **2009**, *113*, 3280–3291.
(69) Yarkony, D. R. *Acc. Chem. Res.* **1998**, *31*, 511–518.
(70) Yarkony, D. R. *J. Phys. Chem. A* **2001**, *105*, 6277–6293.
(71) Muszkat, K. A.; Fischer, E. *J. Chem. Soc. B* **1967**, 662–678.
(72) Lischka, H.; Dallos, M.; Szalay, P. G.; Yarkony, D. R.; Shepard, R. *J. Chem. Phys.* **2004**, *120*, 7322–7329.
(73) Dallos, M.; Lischka, H.; Shepard, R.; Yarkony, D. R.; Szalay, P. G. *J. Chem. Phys.* **2004**, *120*, 7330–7339.
(74) Mori, T.; Kato, S. *Chem. Phys. Lett.* **2009**, *476*, 97–100.
(75) Runge, E.; Gross, E. K. U. *Phys. Rev. Lett.* **1984**, *52*, 997–1000.
(76) Casida, M. E. In *Recent Advances in Density Functional Methods*; Chong, D. P., Ed.; World Scientific: Singapore, 1995; Vol. 1, p 155.
(77) Burke, K.; Werschnik, J.; Gross, E. K. U. *J. Chem. Phys.* **2005**, *123*, 062206−1–062206−9.
(78) Craig, C. F.; Duncan, W. R.; Prezhdo, O. V. *Phys. Rev. Lett.* **2005**, *95*, 163001−1–163001−4.
(79) Tapavicza, E.; Tavernelli, I.; Rothlisberger, U. *Phys. Rev. Lett.* **2007**, *98*, 023001−1–023001−4.
(80) Tapavicza, E.; Tavernelli, I.; Rothlisberger, U.; Filippi, C.; Casida, M. E. *J. Chem. Phys.* **2008**, *129*, 124108−1–124108−19.
(81) Werner, U.; Mitrić, R.; Suzuki, T.; Bonačić-Koutecký, V. *Chem. Phys.* **2008**, *349*, 319–324.
(82) Mitrić, R.; Werner, U.; Bonačić-Koutecký, V. *J. Chem. Phys.* **2008**, *129*, 164118−1–164118−9.
(83) Mitrić, R.; Werner, U.; Wohlgemuth, M.; Seifert, G.; Bonačić-Koutecký, V. *J. Phys. Chem. A* **2009**, *113*, 12700–12705.
(84) Werner, U.; Mitrić, R.; Bonačić-Koutecký, V. *J. Chem. Phys.* **2010**, *132*, 174301−1–174301−8.
(85) Hirai, H.; Sugino, O. *Phys. Chem. Chem. Phys.* **2009**, *11*, 4570–4578.
(86) Levine, B. G.; Ko, C.; Quenneville, J.; Martínez, T. J. *Mol. Phys.* **2006**, *104*, 1039–1051.
(87) Shao, Y.; Head-Gordon, M.; Krylov, A. I. *J. Chem. Phys.* **2003**, *118*, 4807–4818.
(88) Wang, F.; Ziegler, T. *J. Chem. Phys.* **2004**, *121*, 12191–12196.
(89) Wang, F.; Ziegler, T. *J. Chem. Phys.* **2005**, *122*, 074109−1–074109−9.
(90) Vahtras, O.; Rinkevicius, Z. *J. Chem. Phys.* **2007**, *126*, 114101−1–114101−11.
(91) Rinkevicius, Z.; Ågren, H. *Chem. Phys. Lett.* **2010**, *491*, 132–135.
(92) Rinkevicius, Z.; Vahtras, O.; Ågren, H. *J. Chem. Phys.* **2010**, *133*, 114104−1–114104−12.
(93) Slipchenko, L. V.; Krylov, A. I. *J. Chem. Phys.* **2002**, *117* 4694–4708.
(94) Minezawa, N.; Gordon, M. S. *J. Phys. Chem. A* **2009**, *113* 12749–12753.
(95) Huix-Rotllant, M.; Natarajan, B.; Ipatov, A.; Wawire, C. M.; Deutsch, T.; Casida, M. E. *Phys. Chem. Chem. Phys.* **2010**, *12*, 12811–12825.
(96) Levine, B. G.; Coe, J. D.; Martínez, T. J. *J. Phys. Chem. B* **2008**, *112*, 405–413.
(97) Schmidt, M. W.; Baldridge, K. K.; Boatz, J. A.; Elbert, S. T.; Gordon, M. S.; Jensen, J. H.; Koseki, S.; Matsunaga, N.; Nguyen, K. A.; Su, S. J.; Windus, T. L.; Dupuis, M.; Montgomery, J. A., Jr. *J. Comput. Chem.* **1993**, *14*, 1347–1363.
(98) Gordon, M. S.; Schmidt, M. W. In *Theory and Applications of Computational Chemistry: the First Forty Years*; Dykstra, C. E., Frenking, G., Kim, K. S., Scuseria, G. E., Eds.; Elsevier: Amsterdam, The Netherlands, 2005; Chapter 41, pp 1167−1189.
(99) Becke, A. D. *Phys. Rev. A* **1988**, *38*, 3098–3100.
(100) Lee, C.; Yang, W.; Parr, R. G. *Phys. Rev. B* **1988**, *37*, 785–789.
(101) Dunning, T. H., Jr.; Hey, P. J. In *Methods of Electronic Structure Theory*; Schaefer, H. F., III, Ed.; Plenum: New York, 1977.
(102) Traetteberg, M.; Frantsen, E. B.; Mijlhoff, F. C.; Hoekstra, A. *J. Mol. Struct.* **1975**, *26*, 57–68.
(103) Traetteberg, M.; Frantsen, E. B. *J. Mol. Struct.* **1975**, *26*, 69–76.
(104) Champagne, B. B.; Pfanstiel, J. F.; Plusquellic, D. F.; Pratt, D. W.; van Herpen, W. M.; Meerts, W. L. *J. Phys. Chem.* **1990**, *94*, 6–8.
(105) Kwasniewski, S. P.; Claes, L.; François, J.-P.; Deleuze, M. S. *J. Chem. Phys.* **2003**, *118*, 7823–7836 and references therein.
(106) Choi, C. H.; Kertesz, M. *J. Phys. Chem. A* **1997**, *101*, 3823–3831.
(107) Catalán, J. *Chem. Phys. Lett.* **2006**, *421*, 134–137.
(108) Saltiel, J.; Ganapathy, S.; Werking, C. *J. Phys. Chem.* **1987**, *91*, 2755–2758.
(109) Werner, H.-J.; Knowles, P. J.; Lindh, R.; Manby, F. R.; Schütz, M.; Celani, P.; Korona, T.; Mitrushenkov, A.; Rauhut, G.; Adler, T. B.; Amos, R. D.; Bernhardsson, A.; Berning, A.; Cooper, D. L.; Deegan, M. J. O.; Dobbyn, A. J.; Eckert, F.; Goll, E.; Hampel, C.; Hetzer, G.; Hrenar, T.; Knizia, G.; Köppl, C.; Liu, Y.; Lloyd, A. W.; Mata, R. A.; May, A. J.; McNicholas, S. J.; Meyer, W.; Mura, M. E.; Nicklass, A.; Palmieri, P.; Pflüger, K.; Pitzer, R.; Reiher, M.; Schumann, U.; Stoll, H.; Stone, A. J.; Tarroni, R.; Thorsteinsson, T.; Wang, M.; Wolf, A. *MOLPRO*, version 2009.1, a package of ab initio programs; 2009; see http://www.molpro.net.
(110) Oelgemöller, M.; Brem, B.; Frank, R.; Schneider, S.; Lenoir, D.; Hertkorn, N.; Origane, Y.; Lemmen, P.; Lex, J.; Inoue, Y. *J. Chem. Soc., Perkin Trans. 2* **2002**, 1760–1771.
(111) Orlandi, G.; Siebrand, W. *Chem. Phys. Lett.* **1975**, *30*, 352–354.
(112) Negri, F.; Orlandi, G. *J. Phys. Chem.* **1991**, *95*, 748–757.
(113) Wismonski-Knittel, T.; Fischer, G.; Fischer, E. *J. Chem. Soc., Perkin Trans. 2* **1974**, 1930–1940.